

**The importance of high-frequency sea-surface temperature
variability to the intraseasonal oscillation of Indian monsoon
rainfall**

NICHOLAS P. KLINGAMAN*

WALKER INSTITUTE FOR CLIMATE SYSTEM RESEARCH,
DEPARTMENT OF METEOROLOGY, UNIVERSITY OF READING

PETER M. INNESS, JULIA M. SLINGO, HILARY WELLER

WALKER INSTITUTE FOR CLIMATE SYSTEM RESEARCH,
DEPARTMENT OF METEOROLOGY, UNIVERSITY OF READING
AND NATIONAL CENTRE FOR ATMOSPHERIC SCIENCE–CLIMATE

*Corresponding author: Department of Meteorology, University of Reading, Earley Gate, P.O. Box 243, Reading, Berkshire,
RG6 6BB, United Kingdom
E-mail: n.p.klingaman@rdg.ac.uk

ABSTRACT

While the Indian monsoon exhibits substantial variability on interannual timescales, its intraseasonal variability is of greater magnitude and hence of critical importance for predictability of monsoon rains. This intraseasonal variability comprises a 30–50 day northward-propagating oscillation (NPISO) between active and break events of enhanced and reduced rainfall, respectively, over the subcontinent. Several recent studies have implied that coupled general circulation models (CGCMs) were better able to simulate the NPISO than their atmosphere-only counterparts (AGCMs). These studies have forced their AGCM simulations with SSTs from coupled integrations or observations from infrared instruments onboard satellites, both of which substantially underestimate intraseasonal SST variability in the tropical oceans.

We have forced the $1.25^{\circ} \times 0.83^{\circ}$ Hadley Centre Atmospheric Model (HadAM3) with a high-frequency, observed SST dataset from the U.K. Met Office with greater intraseasonal variance in the Indian Ocean than previous products. One ensemble of simulations was forced by daily observed SSTs and a second with monthly means. When compared, the ensemble with daily SSTs displayed significantly greater variability in 30–50 day precipitation across the monsoon domain, variability much more in-line with observations. Individual ensemble members contained intraseasonal events with strength, propagation speed, and organization that closely matched events from a global analysis of precipitation. Even when members from the ensemble with monthly mean SSTs displayed power in intraseasonal rainfall, the events themselves were weak, disorganized, and failed to move northwards from the equator. We conclude that high-frequency SST anomalies not only increased variance in intraseasonal rainfall, but helped to organize and maintain the coherent convective events that comprise the NPISO. Further, our results indicate that an atmosphere-only model can respond to accurate and frequent SST forcing to realistically generate intraseasonal variability. These results have important implications for simulating the NPISO in atmosphere-only and coupled climate models, as well as predicting tropical intraseasonal variability in short- and medium-range weather forecasts.

1. Introduction

a. The northward-propagating intraseasonal oscillation

While the Indian summer monsoon remains one of the most consistent and stable features of the global climate system on interannual and interdecadal timescales, the monsoon's intraseasonal variability (ISV) is far less predictable. Intraseasonal oscillations in the monsoon's strength are dominated by organized convective events that form in the equatorial Indian Ocean (EqIO) and propagate north to the Indian subcontinent (e.g., Annamalai et al. 1999; Annamalai and Slingo 2001). This northward-propagating intraseasonal oscillation (NPISO) has a period of 30–50 days and a speed of approximately 1° latitude day^{-1} (e.g., Yasunari 1979; Krishnamurti and Subrahmanyam 1982; Gadgil 1990; Lawrence and Webster 2002). Convection over India is to some extent anti-correlated with the eastern EqIO (EEqIO), such that “active” periods of enhanced rainfall over the subcontinent are associated with “break” periods of suppressed convection in the EEqIO (Hartmann et al. 1992; Annamalai and Sperber 2005). Waliser et al. (1999a) demonstrated that these recurring active and break events give the monsoon an ISV greater than its interannual variability. Successful long-range prediction of these events would be a great boon to Indian agriculture, primarily for flood and drought mitigation (Webster and Hoyos 2004).

Recent studies have made some progress towards understanding the physical mechanisms underlying the NPISO and its propagation, although competing hypotheses persist. Using observations and simple numerical experiments, Wang and Xie (1997) suggested that the northward propagation was an artifact of an eastward-moving Kelvin-Rossby wave packet that tilted northwest-ward with latitude. Similar efforts have examined reanalysis data and described the meridional propagation as Rossby waves emanating from equatorial convection, although disagreements exist over whether the equatorial convection must first propagate eastward from the western Indian Ocean (Wang and Rui 1990; Annamalai and Slingo 2001; Kemball-Cook and Wang 2001; Lawrence and Webster 2002). If such propagation occurred frequently, it would imply a connection between the NPISO and the Madden-Julian Oscillation (MJO; Madden and Julian 1971, 1972).

Following Madden (1986) and Hendon and Salby (1994), Wang et al. (2005) found that the MJO was too weak and irregular during the monsoon season to sustain the NPISO, instead proposing a self-induction mechanism for the NPISO. While the MJO may coexist and interact with the NPISO, it is unclear whether the MJO forces NPISO events.

b. The effect of air-sea coupling on NPISO simulations

Atmosphere-ocean coupled processes have recently gained support as potential mechanisms for driving the NPISO. Waliser et al. (2003) concluded that all ten atmosphere-only GCMs (AGCMs) from the Climate Variability and Predictability program / Asian-Australian monsoon intercomparison project (Kang et al. 2002) substantially underestimated the monsoon ISV, particularly near the equatorial Indian Ocean, despite displaying reasonable seasonal-mean rainfall. An earlier intercomparison study found that many AGCMs exhibited poor MJO-like variability in northern winter (Slingo et al. 1996). Similar studies with individual AGCMs have confirmed this deficiency (e.g., Rajendran et al. 2002). Still, the fact that AGCMs generated intraseasonal events, albeit weak, suggests that the NPISO is an intrinsically atmospheric mode; the oscillation likely arises from internal atmospheric variability, not coupled processes.

Following many studies that showed air-sea coupling improved simulations of the MJO (e.g., Flatau et al. 1997; Waliser et al. 1999b; Kemball-Cook et al. 2002; Inness and Slingo 2003; Woolnough et al. 2007), recent efforts have focused on the impact of an interactive ocean on the NPISO. These studies are justified by observations of Indian Ocean sea-surface temperatures (SSTs) from the Bay of Bengal Monsoon Experiment (Bhat et al. 2001) and Joint Air-Sea Monsoon Interaction Experiment (Webster et al. 2002) field campaigns, which showed the passage of NPISO events to be associated with substantial SST variations. As in the MJO (Woolnough et al. 2000), anomalous SSTs are out-of-phase with anomalous convection, with warm (cool) SSTs leading enhanced (suppressed) convection by 10–15 days. Anomalies in SST and convection are linked by a negative feedback involving surface heat fluxes, boundary-layer stability, low-level winds, evaporation, and moisture convergence (e.g., Kemball-Cook and Wang 2001; Klingaman et al.

2007).

Fu et al. (2003) compared a hybrid coupled GCM to its atmosphere-only counterpart and found the coupled model produced a strong NPISO with correct phase relationships (compared to observations) between SSTs, convection, and surface heat fluxes. The AGCM produced a weaker NPISO and collocated intense convection with the warmest SSTs, whereas in observations warm SSTs coincide with subsidence, clear skies, and strong insolation (Fu et al. 2002). This error is common in AGCM simulations of intraseasonal behavior in the Indian Ocean and in the west Pacific warm pool. Using the same model, Fu and Wang (2004) demonstrated that coupling substantially improved the two- and three-dimensional structure of the NPISO over an AGCM integration when validated against observations and European Centre for Medium-range Weather Forecasts (ECMWF) analyses. The authors concluded that AGCMs had little hope of ever representing observed monsoon ISV due to their fundamental inability to create and modify the requisite intraseasonal SST anomalies through convective feedbacks.

Rajendran and Kitoh (2006) obtained similar results with the Meteorological Research Institute (MRI) GCM. They found that large-scale atmospheric dynamics could account for the existence of the MJO and the NPISO, but that atmosphere-to-ocean feedbacks amplified the intensity and corrected the phase speed of propagating convection. The MRI coupled GCM reasonably replicated observed phase relationships between rainfall, SST, net surface heat flux, latent heat flux, and surface wind stress, while phase relationships in the AGCM were weaker and temporally distorted. This agrees with Zheng et al. (2004), who employed the coupled model from the Geophysical Fluid Dynamics Laboratory. Fu et al. (2007) demonstrated that a coupled GCM could extend NPISO predictability—as measured by the ratio of signal to forecast-error and by the spatial correlation of anomalies in time-filtered rainfall—by about a week when compared to the same model without an interactive ocean.

Air-sea coupling does not rectify all errors associated with the NPISO. As for the MJO, errors in the mean-state can influence simulations of the NPISO. Inness et al. (2003) showed that reducing systematic errors in the mean state of the Hadley Centre coupled model (HadCM3) could substantially improve simulations of the MJO. Sperber (2004) also suggested that mean state errors could project onto intraseasonal

behavior and so degrade simulations of phenomena such as the MJO and the NPISO. Further, Fu and Wang (2004) noted that model representations of cumulus clouds, interactions between clouds and incident and reflected radiation, boundary-layer processes, and land-surface feedbacks could dramatically affect simulated intraseasonal variability.

c. Motivation

Although many studies have found a weak and inconsistent NPISO in AGCMs, the SST forcing provided to the AGCMs in these studies often has exhibited marked deficiencies. Typically, AGCM simulations have been forced by SSTs from the coupled-model integrations against which the AGCM is to be compared. Fu and Wang (2004), for example, forced their AGCM with the climatological mean SST from their 10 year coupled simulation. Where observed SSTs have been used (e.g., Waliser et al. 2003), they have been taken from the weekly SST analyses produced by the National Centers for Environmental Prediction (NCEP; Reynolds and Smith 1994). When compared to observations, both coupled-model and NCEP SSTs suffer from weak intraseasonal anomalies (Harrison and Vecchi 2001; Senan et al. 2001; Sengupta and Ravichandran 2001; Sengupta et al. 2001).

In a study focused on the west Pacific, Bernie et al. (2005) compared a one-dimensional ocean mixed-layer model to observations from the Intensive Observation Period of the Tropical Ocean Global Atmosphere Coupled Ocean-Atmosphere Response Experiment. They concluded that to capture the intraseasonal SST variability required an ocean model to be forced by diurnally varying heat fluxes and to have a low thermal inertia in the mixed layer, equivalent to a fine vertical resolution. As most coupled climate models used to simulate the NPISO had a top ocean layer on the order of 10 meters thick and were coupled only once per day, the intraseasonal SST anomalies that have been used to force the corresponding AGCM experiments were far too small; Bernie et al. (2005) suggested that a vertical resolution of one meter and three-hourly coupling are required to capture of order 90% of the observed intraseasonal SST variability.

The large errors in these SST products have left unresolved the underlying question of the ability of an

AGCM to simulate the NPISO given reasonably accurate, high-frequency SST forcing. While it is questionable whether an AGCM would simulate the observed phase relationship between anomalous SSTs and convection even with “perfect” SSTs, it may be that realistic SST anomalies could improve the poor ISV in precipitation. Further, an observed SST dataset of high temporal resolution would allow examination of the effect of high-frequency (e.g., daily or weekly) SST anomalies on the NPISO. The tropical sea surface evolves quickly and is tightly coupled to convection and rainfall, so an assessment of the multi-scale interactions of SST and rainfall would be valuable. This type of experiment is possible in an atmosphere-only model, in which SSTs are prescribed and their temporal variability can be controlled. Sensitivity experiments with high-frequency SSTs have been conducted using coupled-model SSTs (Fu and Wang 2004) and the NCEP analysis (Liess and Bengtsson 2004), but given the issues noted above a new experiment with observed SSTs with accurate intraseasonal variability is certainly warranted.

In the absence of a full three-dimensional ocean model proven to predict intraseasonal SST variations of the correct magnitude, we conduct two ensembles of simulations with the Hadley Centre atmosphere model (HadAM3) at high horizontal resolution. These ensembles are forced by a new SST dataset with fine spatial and temporal resolution. Our primary interest is to determine the extent to which high-frequency SST variability influences NPISO-like behavior. To that end, we have forced one HadAM3 ensemble with daily SSTs and the other with monthly means. By comparing simulated NPISO events against observations, this experimental design also allows an investigation of the AGCM’s representation of the NPISO when forced by some of the most-accurate SSTs available. The model and the two ensembles are described in Section 2; we provide the results of our experiments and compare individual ensemble members to observations in Section 3. We discuss the implications of our results concerning high-frequency SSTs, particularly the implications for coupled models and experiments, in Section 4 and summarize our key findings in Section 5.

2. Model and methods

a. The Hadley Centre Atmospheric Model

All experiments in this study were performed with a high-resolution version of the Hadley Centre Atmospheric Model (HadAM3). The model is configured as described in Pope et al. (2000), except that the spatial, vertical, and temporal resolutions have been increased to 1.25° longitude by 0.83° latitude, 30 levels, and 10 minutes, respectively; the spatial resolution is therefore N144L30. Inness et al. (2001) demonstrated that increasing the vertical resolution of HadAM3 from 19 to 30 levels was beneficial to the intraseasonal variability of convection. Similarly, Liess and Bengtsson (2004) found that increasing the vertical resolution of the Hamburg atmospheric model (ECHAM4) from 19 to 30 levels improved the phase speed of the intraseasonal oscillation, and suggested that finer vertical resolution would be particularly important at high horizontal resolutions. Stratton (1999) studied the effect of the N144L30 resolution on the previous version of HadAM (HadAM2b) and concluded that the higher resolution improved the model variability, bringing the model closer to the ECMWF Reanalysis (ERA-40), which uses a similar spatial resolution. Some systematic errors were also reduced, but many (e.g., precipitation) were found to be resolution-independent.

b. Sea-surface temperature forcing

This study is among the first to make use of SST analyses produced by the Global Ocean Data Assimilation Experiment (GODAE) High-Resolution Sea-Surface Temperature (GHRSSST) project (Donlon et al. 2007). GHRSSST provides an assimilation method that combines *in-situ* measurements (e.g., buoys and ships) with those from several microwave and infrared satellites, including the Tropical Rainfall Measuring Mission (TRMM) Microwave Imager (TMI). This study uses the Operational Sea-surface Temperature and sea-Ice Analysis (OSTIA) product from the U.K. National Centre for Ocean Forecasting. The analysis is available daily at $1/20^\circ$ spatial resolution, or approximately 6 km. (Data may be obtained from <http://ghrsstpp.metoffice.com>.) OSTIA is produced through a persistence-based optimal interpolation system (Lorenc

1981) using all data sources available to the GHRSSST project (Donlon et al. 2007).

Due to the novelty of this product, SSTs were available for only one year: February 2005–January 2006. Preliminary comparisons against buoy data indicate that the OSTIA analyses have a root-mean-square error of 0.5°C and a cold bias of 0.15°C at a single point. The high spatial and temporal resolution of this dataset, combined with its use of *in-situ* data and microwave satellites that can estimate SSTs through clouds more accurately than infrared instruments, make the OSTIA analyses far more accurate than the SST datasets frequently used to force atmosphere-only GCMs.

c. Experiment design

We conducted two 30 member ensembles of HadAM3 forced by the OSTIA SST analyses. The first ensemble was forced by the daily OSTIA dataset and so includes high-frequency SST variability; this will be referred to as the “Daily ensemble.” The second ensemble was forced by monthly-mean OSTIA SSTs linearly interpolated to daily values and will be referred to as the “Monthly ensemble.” The monthly-mean SST forcing was calculated using the AMIP II method so that the monthly-mean SSTs in the Daily and Monthly ensembles were equal at every grid point (Taylor et al. 2000). The OSTIA analyses were area-averaged to the HadAM3 spatial resolution and the masking value for sea-ice—used to estimate sea-ice coverage—was altered appropriately to account for the area-averaging. SSTs and sea ice in both ensembles were updated once per day.

The SSTs used to force the Daily ensemble have substantial variability in the 30–70 day intraseasonal band during the monsoon season (June–September, “JJAS” hereafter), particularly in the Bay of Bengal and the Arabian Sea, where values approach 0.5°C (Figure 1a). In the eastern Bay of Bengal the 30–70 day variability accounts for more than 50% of the total SST variability. Variability on the equator is much weaker, but Klingaman et al. (2007) found weak equatorial SST anomalies associated with the northward-propagating intraseasonal oscillation when using TMI SST analyses. The large values off the coast of Africa are due to the spin-up of the Somali Jet at the beginning of the monsoon season, which leads to substantial

coastal upwelling and widespread evaporative sea-surface cooling in June (Webster et al. 1998; Schott and McCreary 2001) that projects onto the 30–70 day timescale. The SSTs used to force the Monthly ensemble have far less intraseasonal variability, as little as one-sixth of the Daily-ensemble SST forcing in the waters surrounding India (Figure 1b). The implications of removing this SST variability will be discussed further in Section 3a.

Within each ensemble, initial conditions were obtained from a previous AMIP II integration of HadAM3 at N144L30 using climatological SSTs. Members were initialized from consecutive days in February from the AMIP II integration, with the validity date of each member’s initial conditions being set to 1 February. All members were then integrated for the year corresponding to the available OSTIA SSTs: 1 February 2005 through 31 January 2006. As the monsoon season begins in June, initializing the simulations in February provides ample spin-up time to allow the model to adjust to the OSTIA SST forcing and for the individual members to diverge.

d. Calculation of ensemble-mean quantities

Where ensemble-mean metrics are used, they have been calculated by first performing the metric on each ensemble member and then taking the mean of the metric across the ensemble. For example, to calculate the ensemble-mean standard deviation of 30–70 day bandpass-filtered JJAS rainfall, we first took the standard deviation of 30–70 day bandpass-filtered JJAS rainfall from each member and then computed the mean of that variance across the ensemble.

3. Impacts of high-frequency SSTs

a. Ensemble-mean diagnostics

When forced by daily OSTIA SSTs, HadAM3 reproduced well the JJAS-mean rainfall across the monsoon domain, with local maxima in the northern Bay of Bay of Bengal, along the hilly western coast of India,

and in the Indian Ocean south of the equator (Figure 2a). The model's spatial distribution of rainfall across India resembled to a high degree the $1^\circ \times 1^\circ$ gridded 1951–2004 climatology of JJAS rainfall compiled by the Indian Meteorological Department (Figure 2b; Rajeevan et al. 2005). The model underestimated the rainfall near the southwest tip of India; produced a weaker rain-shadow effect from the western mountains, resulting in wet biases over central southern India; and overestimated rainfall in the northeastern and northern regions of the subcontinent.

The difference between the Daily and Monthly ensembles gives the impact of including submonthly SST variability in the forcing dataset. Submonthly SST variability caused small but statistically significant changes in ensemble-mean, JJAS-mean precipitation. The Daily ensemble showed higher seasonal-mean rainfall over the northern Bay of Bengal and the Arabian Sea and less rainfall to the south of the peninsula (Figure 2c). These differences occurred even though the SST forcing for both ensembles had the same monthly—and hence seasonal—mean at each gridpoint. Furthermore, the differences were negative as well as positive, which suggests that they were likely not caused by the non-linear response of precipitation to SSTs (i.e., through the Clausius-Clapeyron relationship), but may be associated with circulation changes. While the statistical significance of the changes to the ensemble-mean, JJAS-mean rainfall is a noteworthy result, the low magnitude of these changes implies that including submonthly SST variability did not substantially alter the model climatology from the Monthly ensemble.

An increase in the monsoon intraseasonal variability in the Daily ensemble was immediately detectable when precipitation was filtered to intraseasonal timescales (30–70 days; Figure 2d). These increases are mostly confined to the ocean, although some more-scattered significant values can be seen across northwestern and central India. The increased intraseasonal variability across the eastern Indian Ocean and northwards into the Bay of Bengal are particularly encouraging for the NPISO, as past studies have indicated that the oscillation was more clearly observable in the eastern basin (Lawrence and Webster 2002; Klingaman et al. 2007).

When area-averaged precipitation over the Indian landmass was examined, substantial differences were obtained between the ensemble means across the subcontinent (Figure 3; the red lines are the ensemble

means). Both ensembles reasonably simulated the evolution of the daily climatology from the all-India rainfall dataset provided by the Indian Institute for Tropical Meteorology, although with a persistent wet bias of several millimeters per day. On qualitative inspection, however, the Daily ensemble-mean displayed clear intraseasonal variability, particularly after July 1 (Figure 3a). One active-break-active cycle began with an active event in late July, followed by break conditions during most of August and then a return to active conditions in early September. Most of the individual ensemble members (black lines) mimicked the ensemble mean through this oscillation. However, no ensemble member reliably simulated the observed all-India rainfall for 2005 (green line), the same year as the SST forcing. That season was characterized by a MJO-like equatorial convection in May and a delayed onset of monsoon rains across India; during June the observed rainfall lay outside the range of both ensembles. This suggests that the conditions influencing the delayed onset either had no significant impact on the SSTs—and so are not present in the OSTIA analyses—or cannot be driven in this model from forced SSTs.

Further evidence for the ability of submonthly SSTs to affect intraseasonal monsoon behavior came from the ensemble-mean wavelet transform of precipitation in the northern Bay of Bengal, the region that showed one of the largest increases in 30–70 bandpass-filtered precipitation in the Daily ensemble (Figure 2b). The wavelet analysis from the Daily ensemble confirmed that including daily SST variability induces additional variance in intraseasonal rainfall, particularly at periods between 20 and 50 days (Figure 4a). This is the characteristic period of the northward-propagating oscillation and so suggests that the oscillation might be better-resolved in the Daily ensemble. In this band, the Daily ensemble had power exceeding the 95% confidence level (against a background red-noise spectrum) beginning in late July, with power exceeding 90% confidence extending back to early July. In striking contrast, the Monthly ensemble had no power at intraseasonal periods exceeding any reasonable confidence level at any time during the monsoon season (Figure 4b). We qualitatively examined the wavelet transforms from each ensemble member (not shown) and found that the majority of the Daily-ensemble members contained significant power above 90% confidence in the 20–50 day band during the season, while the majority of the Monthly-ensemble members did not. The limited temporal extent of the statistically significant power at periods shorter than 10 days suggests

that this power is probably associated with sharp changes in the seasonal cycle of precipitation rather than with persistent variability. Comparing the dates of this high-frequency power with the timeseries of all-India precipitation (Figure 3) supports this hypothesis, as the ensemble-mean precipitation decreased rapidly in late July and increased again in early September. These changes projected onto short-frequency wavelets and appeared in the wavelet analysis as statistically significant power.

The wavelet transforms of the forcing SSTs in the Bay of Bengal indicate that the Daily SST forcing contained statistically significant power in the 30–50 day band during late July, August, and September (Figure 4c), a period which broadly corresponds to the occurrence of power in precipitation at the 95% confidence level in Figure 4a. In taking the monthly means of these SSTs, we have removed all power at periods shorter than 30 days and damped variability down to at least 60-day periods (Figure 4d). The association between the intraseasonal variance in SSTs and rainfall demonstrates the potential for a strong link between SSTs and precipitation in this region.

To explore the quantitative difference in intraseasonal activity across all ensemble members, we have constructed a metric that considers the power on those timescales. For each member, we took the area-averaged precipitation for each day in the same region used to construct Figure 4 and performed a one-dimensional wavelet transform on the resulting timeseries. Since we were most interested in the intraseasonal periods where the Daily ensemble showed statistically significant power, we considered only periods between 30 and 50 days; periods between 20 and 30 days were not considered so as to clearly separate the 30–50 day NPISO from 10–20 day variability along the monsoon trough (Annamalai and Slingo 2001). We normalized the power at each period in the 30–50 day range by the 90% confidence level for that particular period.¹ The normalization ensured that longer periods—which have greater power, but also a greater confidence threshold from the red-noise spectrum—do not carry greater weight than shorter periods. All values greater than unity (i.e., for which the power exceeded 90% confidence) were summed across JJAS. Therefore, this “intraseasonal-power metric” provides a measure of both the frequency of occurrence and

¹Performing this same analysis with the 95% confidence limit generated similar results to those described below, but with lower values for all ensemble members since fewer points have power exceeding 95% confidence.

the intensity of power in the 30–50 day band in each ensemble member.

We calculated the intraseasonal-power metric on each member in both ensembles and for the 1997–2006 $1^\circ \times 1^\circ$ gridded, daily precipitation analyses from the Global Precipitation Climatology Project (GPCP). The high spatial and temporal resolutions of the GPCP data nearly match the resolutions of the HadAM3 simulations. The probability density function (PDF) of the intraseasonal-power metric values confirms that the vast majority of members in the Daily ensemble had greater 30–50 day power in precipitation than their counterparts in the Monthly ensemble (Figure 5). By this metric, most of the members in the Monthly ensemble had very little statistically significant intraseasonal power in Bay of Bengal rainfall compared to the GPCP analysis. On the other hand, the PDF of the Daily ensemble approximated the GPCP PDF well. If one were to choose an ensemble member at random from each ensemble, the Daily ensemble member would be about twice as likely to have intraseasonal variability close to the GPCP analysis from 2005, the same year as the OSTIA SSTs used to force the HadAM3 simulations.

An increase in significant power at intraseasonal frequencies is a necessary, but not a sufficient condition for an improved NPISO in the Daily ensemble. While the increase in power from introducing submonthly SSTs is a noteworthy result in itself, individual intraseasonal events must display coherent northward propagation if we are to conclude that the additional intraseasonal SST forcing improved the NPISO in these atmosphere-only simulations. To assess the spatial coherence of the increase in intraseasonal variability, we performed wavelet transforms similar to those in Figure 4 for each ensemble member at every gridpoint in the monsoon domain. From these wavelet transforms, we calculated the decimal fraction of times during JJAS that the power in precipitation at each period in the 30–50 day band exceeded the 90% confidence level. This is similar to the intraseasonal-power metric, but here we are not concerned with the margin by which the power exceeds 90% confidence, only that the power does exceed that level; it is essentially a measure of the frequency of statistically significant intraseasonal power at each gridpoint. One would expect a strong, coherent NPISO to appear as a solid band of higher values, allowing one trace the propagation of the NPISO in the model. The result (not shown) mimicked the pattern of increased intraseasonal variability in the Daily ensemble shown in Figure 2d. With few exceptions, values for the Daily ensemble were higher than those

for the Monthly ensemble across the monsoon domain, indicating that the increase in intraseasonal power seen in Figure 4a was not confined to the northern Bay of Bengal. Statistically significant intraseasonal power was therefore far more frequent in the Daily ensemble, particularly in the eastern third of the basin.

b. Model NPISO events compared with GPCP analysis

Having determined that the Daily ensemble contained greater intraseasonal variability and possibly a stronger NPISO than the Monthly ensemble, we must now consider whether the modeled NPISO in the Daily ensemble more-closely resembles the observed NPISO. First, it is important to note that providing daily, observed SST forcing did not correct a common error in AGCM simulations of intraseasonal monsoon variability: the phase relationship between SST anomalies and atmospheric deep convection. We computed the correlation between the linear trend in longitude-averaged (80–90°E) rainfall and SST over JJAS across all ensemble members; the trend was calculated using a centered 11-day window at each day. We chose this band because it contains little land south of 25°N; the NPISO is strongest in the eastern third of the Indian Ocean; and both ensembles had some of their highest frequencies of occurrence of intraseasonal power in this band. The linear trend in rainfall is a far more useful diagnostic than the raw rainfall timeseries because of the strong latitudinal gradient in climatological precipitation between the equator and the Indian subcontinent in JJAS. We elected to use the 11 day trend so as to obtain sufficient data points to calculate a useful diagnostic, while limiting the mixing of intraseasonal modes. The “ensemble-mean” lag-correlation coefficients were calculated by taking the mean of the lag covariances from the individual members, then dividing by the product of the standard deviations of timeseries created by concatenating data from all 30 ensemble members. To account for the serial correlations in precipitation within each ensemble member, degrees of freedom were estimated using the method of Livezey and Chen (1983).

In the Daily ensemble and north of the equator, SSTs were most-strongly correlated with rainfall at within a day or two of zero lag (Figure 6a), consistent with many previous AGCM studies (e.g., Fu and Wang 2004; Rajendran and Kitoh 2006). The Monthly ensemble used daily SSTs from a linear interpolation

between monthly means, and so correlating the trends in rainfall and SST produces no signal (Figure 6b). Correlating the trends in GPCP rainfall and TMI SSTs over 1998-2006 demonstrates that, in analysis, SSTs warmed most strongly 8–10 days before the maximum increase in rainfall, then cooled most strongly 8–10 days after (Figure 6c). This suggests a shorter timescale for atmosphere-ocean interactions than Fu and Wang (2004), which used different observed datasets, a wider band for longitude averaging, and a 20–70 day bandpass filter.

Even without the correct phase relationship between SSTs and deep convection, an AGCM may still be able to simulate an NPISO with reasonable intensity and propagation speed if the atmosphere responds to warm SST anomalies by generating organized convection. If the SST anomalies have a realistic magnitude and propagate northwards—as they do in observations of the NPISO (e.g., Klingaman et al. 2007)—they may be able to induce the convection to follow. To diagnose this behavior in our ensembles, we used the same linear trend in rainfall as in Figure 6. In the ensemble-mean rainfall trend, the Daily ensemble had stronger and substantially more-coherent intraseasonal events than the Monthly ensemble (Figures 7a and 7b). Active and break events in the Daily ensemble-mean trend propagated northwards from at least 10°N with a phase speed either consistent with or faster than the events in the GPCP analyses and previous studies using observations. The Monthly ensemble-mean trend showed little or no northward propagation and contained no events as strong as those in the Daily ensemble-mean.

It may be, however, that the intraseasonal variability of the Monthly ensemble-mean was dampened by variability in the timing of intraseasonal events in the individual members. In other words, if each member of the Monthly ensemble contained substantial active and break events but at different times during the monsoon season, the ensemble-mean would falsely indicate that no active or break events occurred in the Monthly ensemble. From the 30 members in each ensemble, we selected three members to examine more closely, to determine if the individual simulations demonstrated the same behavior as the ensemble-mean. We chose the three members from the ensemble that had values of the intraseasonal-power metric closest to the most-probable value, determined from the PDF for that ensemble (i.e., the peak of the curves in Figure 5). We refer to these as the “typical members” from each ensemble.

The typical members confirmed that the Daily ensemble not only has greater intraseasonal rainfall variability but also a far greater organization to its convective events. The three Daily typical members (Figures 7c, 7e, and 7g) demonstrated consistent, northward-propagating increases and decreases in rainfall throughout the monsoon season, while the Monthly typical members (Figures 7d, 7f, and 7h) had far less coherence to their limited variability. The Daily members and ensemble mean produced intraseasonal events at approximately the same times as the 2005 GPCP data (Figure 7i)—beginning from the equator near 1 July and 1 September—which suggests that these events are connected to the SSTs, since the 2005 OSTIA analyses forced the simulations. The fact that the events were shifted earlier by 8–10 days in the simulations supports this hypothesis, since this was the discrepancy between the model and observations in the phase relationship between SSTs and rainfall (Figure 6). Thus the warming trend in SSTs that has been observed to precede an active event is coincident with an active event in HadAM3, while the cooling SSTs that precede a break event in observations is coincident with a break event in the model; the model is half a cycle out of phase with observations.

It is interesting to note the southward propagation from the equator that is occasionally seen in the model simulations (particularly Figure 7g) and in the September event in the GPCP data. Several previous studies (e.g., Lawrence and Webster 2002) have suggested that equatorial convection could generate equatorially symmetric Rossby cells, of which the Northern-Hemisphere cell would be amplified by the northern-summer basic state. While the weaker Southern-Hemisphere cell was not consistently detectable in either ensemble or the GPCP analysis, the equatorial symmetry seen in some events in Figure 7 implies that such a mechanism might exist in those simulations.

To further examine the northward propagation of organized convective events in each ensemble, we computed the lead-lag correlations of 30–50 day bandpass-filtered longitude-averaged (85–90°E) rainfall during the monsoon season. Longitude-averaged rainfall at each latitude point was correlated with the time-series of longitude-averaged rainfall at 20°N. This northern latitude was chosen for the base point because while some ensemble members have limited northward propagation, almost all members demonstrated some 30–50 day variability in precipitation in the northern Bay of Bengal. This can be seen in Figure 2d, where

the increase in intraseasonal variability of precipitation was greater over the Bay of Bengal than over the eastern equatorial Indian Ocean. Selecting a northerly latitude for the base point therefore provided the best opportunity to detect any latitudinal propagation in the intraseasonal events.

The Daily ensemble-mean lead-lag correlation showed statistically significant (at the 5% level) northward propagation from 5°N at a lead of about 20 days before the precipitation reached 20°N (Figure 8a). The opposite phase of the oscillation occurred 20–25 days later and displayed a similar northward track. By contrast, the Monthly ensemble-mean showed no statistically significant, coherent northward propagation for any event (Figure 8b). When the typical members from each ensemble were considered, the Daily typical members demonstrated northward propagation from at least 10°N (Figures 8c, 8e, 8g), with two of the members also showing southward propagation from the equator. These three members and the ensemble mean all showed a propagation speed of about 1° day^{-1} from 10°N, in line with observations (Yasunari 1979; Krishnamurti and Subrahmanyam 1982). Combined with the similar timing of intraseasonal events seen in Figure 7, this behavior suggests that in some cases an atmosphere-only model can respond to high-frequency sea-surface temperature forcing to produce an intraseasonal oscillation that resembles observations in intensity, speed, and timing. On the other hand, the Monthly typical members exhibited no clear northward propagation; they completely failed to produce any signal resembling an organized intraseasonal convective event (Figures 8d, 8f, and 8h).

In the lag-correlations of daily typical members, the ensemble mean and in observations, the signal of an intraseasonal oscillation was often found first in the north (i.e., over India) followed by the opposite phase forming in the south (i.e., over the eastern equatorial Indian Ocean). This implies that intraseasonal monsoon rainfall cannot be predicted solely from events propagating from the south; intraseasonal rainfall over India displays the greatest predictability once either an active or a break event has reached the subcontinent itself.

While the typical members from each ensemble represented the most-probable amounts of intraseasonal variability one could obtain from that ensemble, the typical members from the Daily ensemble contained substantially more of that variability than the typical members from the Monthly ensemble. Comparing the typical members from each ensemble has shown that the Daily ensemble was far more likely to pro-

duce organized, northward-propagating intraseasonal events, but it did not prove that the Monthly ensemble was incapable of doing so as well. The Monthly ensemble did contain some members with values of the intraseasonal-power metric that were equal to or higher than many members from the Daily ensemble (Figure 5), and these Monthly-ensemble members may well show an organized NPISO similar to their Daily-ensemble counterparts.

To test this hypothesis, we compared the three members from each ensemble that had a value of the intraseasonal-power metric that was closest to the value for the 2005 GPCP analysis (approximately 650); these will be referred to as the “observational members.” This not only created a like-with-like comparison between the two ensembles in terms of intraseasonal power, but also between the ensemble members and the GPCP data. We repeated the diagnostics of the 11 day centered linear trend in rainfall (Figure 9) and the lead-lag correlations of 30–50 day rainfall with a base point at 20°N (Figure 10). As before, the members from the Daily ensemble displayed more-intense and more-coherent NPISO-like events than the corresponding members from the Monthly ensembles. The trend in rainfall showed several strong events in the Daily observational member in July and September with timing similar to the GPCP analyses (Figure 7g), as for the typical members from the Daily ensemble. Intraseasonal events in the Monthly ensemble member are scattered at best and rarely extended south of 15°N. The lead-lag correlations also demonstrated that the Daily ensemble members had more-frequent movement of convection from the equatorial Indian Ocean to the subcontinent, while only one of the Monthly ensemble members showed any latitudinal propagation in its intraseasonal variability (Figure 10b).

The results of Figures 9 and 10 are particularly remarkable since here we have compared members from each ensemble that have similar amounts of intraseasonal variability. This indicates that even when the Monthly ensemble members managed to generate substantial power in 30–50 day precipitation, the spatio-temporal pattern of precipitation did not resemble the northward-propagating oscillation. The members chosen had high values of the intraseasonal-power metric, higher than the values of the typical members from either ensemble. While the Monthly ensemble could not generate NPISO-like events with even an high (for that ensemble) amount of intraseasonal power, the typical members from the Daily ensemble

produced intense northward-propagating events that in some cases very closely resembled observations. This speaks to the ability of high-frequency SSTs to not only generate greater intraseasonal variability in rainfall, but to organize convective events and encourage their northward propagation towards the Indian landmass. High-frequency SST variations are thus a critical component of monsoon active-break cycles.

4. Discussion

Studies that have investigated the ability of atmosphere-only models to simulate the intraseasonal variability of the Indian monsoon have suggested, without exception, that AGCMs contain NPISO-like variability but cannot reproduce either the strength or propagation speed of the oscillation (e.g., Fu et al. 2003; Waliser et al. 2003; Fu and Wang 2004; Rajendran and Kitoh 2006). Those studies that have also employed coupled models have found that air-sea coupling improved representations of the NPISO. The first result led to the conclusion that the NPISO is an internal atmospheric mode, while the second implied that atmosphere-ocean feedbacks were essential to generate a strong NPISO with the appropriate meridional velocity. Our results support this hypothesis, as some of the Monthly ensemble members contain intraseasonal variability that agrees with GPCP analyses (Figure 5 and Figure 7j). These studies considered the key failing of AGCMs to be their inability to represent the near-quadrature phase relationship between sea-surface temperatures and convection. We noted in Section 1c, however, that all previous studies to simulate the NPISO with an AGCM have employed SST forcing that substantially underestimates the intraseasonal SST anomalies associated with individual active and break events.

Here, we have demonstrated that an AGCM can reproduce NPISO-like variability with greater fidelity if forced by SSTs with more-realistic intraseasonal variability (ISV), even though the phase relationship between rainfall and SST remains incorrect (Figure 6). In reality, the high-frequency SST variability in the monsoon region is undoubtedly a response to the high-frequency atmospheric forcing. The caveat in our simulations, then, is that incorrect physical responses may occur if the atmosphere is substantially “out of sync” with the SST forcing. In other words, the atmosphere is not a forced system and so individual

ensemble members may show widely varying responses given the same SST forcing, some of which may not be realistic. This is likely why some of the members of the Daily ensemble showed little or no intraseasonal variability (Figure 5).

It is reasonable to conclude, therefore, that is not necessarily the zero-lag phase relationship between the SSTs and convection that resulted in weak NPISO-like variability in past AGCM experiments, but the low magnitude of daily, submonthly, and intraseasonal SST variability in the forcing SSTs. For instance, using coupled-model SSTs, Fu and Wang (2004) found little improvement between AGCM experiments with monthly mean and daily SST forcing. Combined with the results in this study, this suggests that not only are the frequency of the SST anomalies critical for an accurate simulation of the NPISO, but also the magnitude of the SST anomalies on submonthly timescales. It could be argued that without atmosphere-to-ocean feedbacks our modeled NPISO events may not have been driven by entirely correct physical mechanisms, but their very existence speaks to the ability of an AGCM to respond to spatially coherent and accurate intraseasonal SST anomalies with organized intraseasonal convection.

The results of this study have clear implications for future ACGM and coupled-model experiments. Simulations which remove or under-represent high-frequency SST anomalies severely limit the ability of the model to reproduce an NPISO that resembles observations in frequency, intensity, and propagation speed. This is equally true for coupled models with dynamic SSTs as for atmosphere-only simulations. As previously mentioned in Section 1c, many coupled models substantially underestimate SST variability due to excessively high thermal inertia, a function of coarse vertical resolution in the upper ocean. Our results indicate that this vertical resolution must be improved if representations—and hence predictability—of the NPISO are to be improved, as has also been demonstrated by Bernie et al. (2007) for the MJO. Similarly, atmosphere-only simulations which continue to use monthly mean SST forcing are imposing an unnecessary constraint on the ability of the model to generate organized convection in response to high-frequency SST anomalies.

Further, our experiments suggest that including high-frequency, realistic SST anomalies are necessary for capturing the initiation and northward propagation of NPISO events in an AGCM. Thus, the predictabil-

ity of active and break events in such a model must be in part a function of the accuracy of these anomalies. Fu et al. (2007) recently showed an increase in the NPISO predictability timescale of nearly one week in a coupled model over an AGCM. Many short- and medium-range weather prediction models, however, are AGCMs with persistent SST anomalies. Without either an interactive ocean or a technique for adding high-frequency SST perturbations, these models will likely fail to predict the frequency and intensity of NPISO events. In this case, an interactive ocean need not be more than a mixed-layer scheme (e.g., Woolnough et al. 2007), as the response of the Indian Ocean on intraseasonal timescales is likely to be dominated by thermodynamic processes. Future work will examine the impact of adding a mixed-layer scheme to an AGCM on NPISO predictability.

5. Summary and Conclusions

Our ensembles of HadAM3 simulations forced with OSTIA SSTs demonstrated that an AGCM could respond to accurate, high-frequency SST forcing to organize convection and generate NPISO-like variability. We noted in Section 3a that the members of the Daily ensemble contained substantially more power in 30–50 day precipitation than the members from the Monthly ensemble. Figure 5 demonstrated this conclusively; it also showed that the Daily ensemble matches the GPCP analysis remarkably well. Not all members of the Daily ensemble contained appropriate amounts of intraseasonal power, but the inclusion of realistic, daily SST anomalies allowed more ensemble members to contain this power than in the Monthly ensemble. The key result here, then, is that while HadAM3 did not always respond to daily SST forcing by organizing NPISO-like variability in convection, the daily SST forcing significantly improved the chances that an individual ensemble member would produce such variability (over monthly mean SST forcing).

Not only did the members of the Daily ensemble reproduce accurate intraseasonal precipitation variability twice as frequently than the Monthly-ensemble members, but those that showed an organization and propagation to the convection that resembled the NPISO in the GPCP analyses. Even when an integration forced with monthly mean SSTs produced substantial intraseasonal variability in precipitation, this was not

organized into a coherent, northward-propagating NPISO event. Taken together, these results and those from the previous paragraph indicate that daily SST forcing can induce an atmosphere-only model to produce accurate amounts of 30–50 day power in precipitation far more frequently than monthly mean SST forcing, and to organize that variability into coherent convective events that move northwards with a phase speed that agrees with the NPISO.

Even with accurate, daily SST forcing, our AGCM still collocated the rainfall too readily over the warmest sea-surface temperatures (Figure 6). This is in direct contrast with observations, which have consistently shown that the strongest convection is associated with cooling SSTs; warm SSTs are associated with NPISO break events and suppressed convection (e.g., Fu and Wang 2004; Klingaman et al. 2007). The incorrect phase relationship is likely due to the lack of feedbacks between convection and the ocean surface, which is an intrinsic failure of atmosphere-only models when simulating tropical intraseasonal variability and which cannot be resolved by improving the SST forcing. It is also possible that this failure is due to the HadAM3 convection scheme responding too readily to the warm SSTs. Our results indicate that a coupled model must be able to accurately represent the high-frequency SST anomalies that are so critical to the intraseasonal variability of convection and precipitation. High-frequency SSTs play a key role in strengthening and maintaining the NPISO and so cannot be neglected, regardless of whether they are being forced in a atmosphere-only model or simulated in a coupled one.

Acknowledgments.

NPK is supported by a grant from the Marshall Aid Commemoration Commission. PMI, JMS, and HW are supported by the National Centre for Atmospheric Science, a Natural Environment Research Council Collaborative Centre. The authors would like to thank Mr. John Stark of the Hadley Centre at the United Kingdom Met Office for his assistance in obtaining the OSTIA data.

REFERENCES

- Annamalai, H. and J. M. Slingo, 2001: Active/break cycles: diagnosis of the intraseasonal variability of the Asian Summer Monsoon. *Clim. Dynam.*, **18**, 85–102.
- Annamalai, H., J. M. Slingo, K. R. Sperber, and K. Hodges, 1999: The mean evolution and variability of the asian summer monsoon: Comparison of ECMWF and NCEP/NCAR Reanalyses. *Mon. Weather Rev.*, **127**, 1157–1186.
- Annamalai, H. and K. R. Sperber, 2005: Regional heat sources and the active and break phases of Boreal Summer Intraseasonal Variability. *J. Atmos. Sci.*, **62**, 2726–2748.
- Bernie, D. J., E. Guilyardi, G. Madec, J. M. Slingo, and S. J. Woolnough, 2007: Impact of resolving the diurnal cycle in an ocean-atmosphere GCM. Part 1: a diurnally forced GCM. *Clim. Dynam.*, **29**, 575–590.
- Bernie, D. J., S. J. Woolnough, and J. M. Slingo, 2005: Modeling diurnal and intraseasonal variability of the ocean mixed layer. *J. Climate*, **18**, 1190–1202.
- Bhat, G. S., S. Gadgil, P. V. Hareesh Kumar, S. R. Kalsi, P. Madhusoodanan, V. S. N. Murty, C. V. K. Prasada Rao, V. Ramesh Babu, L. V. G. Rao, R. R. Rao, M. Ravichandran, K. G. Reddy, P. Sanjeeva Rao, D. Sengupta, D. R. Sikka, J. Swain, and P. N. Vinayachandran, 2001: BOBMEX: The Bay of Bengal Monsoon Experiment. *Bull. Amer. Meteorol. Soc.*, **82**, 2217–2243.
- Donlon, C., I. Robinson, K. S. Casey, J. Vazquez-Cuervo, E. Armstrong, O. Arino, G. C., D. May, P. LeBorgne, J. Piolle, I. Barton, H. Beggs, D. J. S. Poulter, C. J. Merchant, A. Bingham, S. Heinz, A. Harris, G. Wick, B. Emery, P. Minnett, R. Evans, D. Llewellyn-Jones, C. Mutlow, R. W. Reynolds, H. Kawamura, and N. Rayner, 2007: The Global Ocean Data Assimilation Experiment High-resolution Sea Surface Temperature Pilot Project. *Bull. Amer. Meteorol. Soc.*, **88**, 1197–1213.

- Flatau, M., P. J. Flatau, P. Phoebus, and P. P. Niler, 1997: The feedback between equatorial convection and local radiative and evaporative processes: The implications for intraseasonal oscillations. *J. Atmos. Sci.*, **54**, 2373–2386.
- Fu, X. and B. Wang, 2004: The boreal-summer intraseasonal oscillations simulated in a hybrid coupled atmosphere-ocean model. *Mon. Weather Rev.*, **132**, 2628–2649.
- Fu, X., B. Wang, and T. Li, 2002: Impacts of air-sea coupling on the simulation of mean asian summer monsoon in echam4 model. *Mon. Weather Rev.*, **130**, 2889–2903.
- Fu, X., B. Wang, T. Li, and J. P. McCreary, 2003: Coupling between northward-propagating, intraseasonal oscillations and sea surface temperature in the Indian Ocean. *J. Atmos. Sci.*, **60**, 1733–1753.
- Fu, X., B. Wang, D. E. Waliser, and L. Tao, 2007: Impact of atmosphere-ocean coupling on the predictability of monsoon intraseasonal oscillations. *J. Atmos. Sci.*, **64**, 157–174.
- Gadgil, S., 1990: Poleward propagation of the ITCZ: Observations and theory. *Mausam*, **41**, 285–290.
- Harrison, D. E. and G. A. Vecchi, 2001: January 1999 Indian Ocean cooling event. *Geophys. Res. Lett.*, **28** (19), 3717–3720.
- Hartmann, D. L., M. L. Michelsen, and S. A. Klein, 1992: Seasonal variations of tropical intraseasonal oscillations: A 20–25 day oscillation in the western Pacific. *J. Atmos. Sci.*, **49**, 1277–1289.
- Hendon, H. and M. L. Salby, 1994: The life cycle of the Madden-Julian oscillation. *J. Atmos. Sci.*, **51**, 2225–2237.
- Inness, P. M. and J. M. Slingo, 2003: Simulation of the Madden-Julian oscillation in a coupled general circulation model. Part I: Comparison with observations and an atmosphere-only GCM. *J. Climate*, **16**, 345–364.
- Inness, P. M., J. M. Slingo, E. Guilyardi, and J. Cole, 2001: Organization of tropical convection in a GCM

- with varying vertical resolution: Implications for the simulation of the Madden-Julian Oscillation. *Clim. Dynam.*, **17**, 777–793.
- , 2003: Simulation of the Madden-Julian oscillation in a coupled general circulation model. Part II: The role of the basic state. *J. Climate*, **17**, 365–382.
- Kang, I., K. Jin, B. Wang, K. M. Lau, J. Shukla, V. Krishnamurthy, S. D. Schubert, D. E. Waliser, W. F. Stern, A. Kitoh, G. A. Meehl, M. Kanamitsu, V. Y. Galin, V. Satyan, C. K. Park, and Y. Liu, 2002: Intercomparisons of the climatological variations of asian summer monsoon precipitation simulation by 10 GCMs. *Clim. Dynam.*, **19**, 383–395.
- Kemball-Cook, S. and B. Wang, 2001: Equatorial waves and air-sea interaction in the Boreal Summer Intraseasonal Oscillation. *J. Climate*, **14**, 2923–2942.
- Kemball-Cook, S., B. Wang, and X. Fu, 2002: Simulation of the ISO in the ECHAM4 model: The impact of coupling with an ocean model. *J. Atmos. Sci.*, **59**, 1433–1453.
- Klingaman, N. P., H. Weller, J. M. Slingo, and P. M. Inness, 2007: The intraseasonal variability of the indian summer monsoon using TMI sea-surface temperatures and ECMWF reanalysis. *J. Climate. In press.*
- Krishnamurti, T. N. and D. Subrahmanyam, 1982: The 30–50 day mode at 850 mb during MONEX. *J. Atmos. Sci.*, **39**, 2088–2095.
- Lawrence, D. M. and P. J. Webster, 2002: The Boreal Intraseasonal Oscillation: Relationship between Northward and Eastward Movement of Convection. *J. Climate*, **59**, 1593–1606.
- Liess, S. and S. Bengtsson, 2004: The intraseasonal oscillation in ECHAM4 Part II: Sensitivity studies. *Clim. Dynam.*, **22**, 671–688.
- Livezey, R. E. and W. E. Chen, 1983: Statistical field significance and its determination by Monte Carlo techniques. *Mon. Weather Rev.*, **111**, 46–59.

- Lorenc, A. C., 1981: A global three-dimensional multi-variate statistical interpolation scheme. *Mon. Weather Rev.*, **109**, 701–721.
- Madden, R. A., 1986: Seasonal variations of the 40–50 day oscillation in the Tropics. *J. Atmos. Sci.*, **43**, 3138–3158.
- Madden, R. A. and P. R. Julian, 1971: Detection of a 40–50 day oscillation in the zonal wind in the tropical Pacific. *J. Atmos. Sci.*, **28**, 702–708.
- , 1972: Description of global-scale circulation cells in the Tropics with a 40–50 day period. *J. Atmos. Sci.*, **29**, 1109–1123.
- Pope, V. D., M. L. Gallani, P. R. Rowntree, and R. A. Stratton, 2000: The impact of the new physical parameterizations in the hadley centre climate model. *Clim. Dynam.*, **16**, 123–146.
- Rajeevan, M., J. Bhate, J. D. Kale, and B. Lal, 2005: High resolution daily gridded rainfall data the Indian region: Analysis of break and active monsoon spells. *Curr. Sci. India*, **91**, 296–306.
- Rajendran, K. and A. Kitoh, 2006: Modulation of tropical intraseasonal oscillations by atmosphere-ocean coupling. *J. Climate*, **19**, 366–391.
- Rajendran, K., R. S. Nanjundiah, and J. Srinivasan, 2002: The impact of surface hydrology on the simulation of tropical intraseasonal oscillation in NCAR (CCM2) atmospheric GCM. *J. Meteor. Soc. Japan*, **80**, 1357–1381.
- Reynolds, R. W. and T. M. Smith, 1994: Improved global sea surface temperature analyses using optimum interpolation. *J. Climate*, **7**, 929–948.
- Schott, F. A. and J. P. McCreary, 2001: The monsoon circulation of the Indian Ocean. *Progress in Oceanography*, **51**, 1–123.
- Senan, R., A. D. S., and D. Sengupta, 2001: Validation of SST and windspeed from TRMM using North

- Indian Ocean moored buoy observations. Technical Report CAOS Report 2001AS1, Centre for Atmospheric and Oceanic Sciences, Indian Institute of Science, Bangalore, India.
- Sengupta, D., B. N. Goswami, and R. Senan, 2001: Coherent intraseasonal oscillations of ocean and atmosphere during the Asian Summer Monsoon. *Geophys. Res. Lett.*, **20**, 4127–4130.
- Sengupta, D. and M. Ravichandran, 2001: Oscillations of the Bay of Bengal sea surface temperature during the 1998 summer monsoon. *Geophys. Res. Lett.*, **28**, 2033–2036.
- Slingo, J. M., K. R. Sperber, J. S. Boyle, J. P. Ceron, M. Dix, B. Dugas, W. Ebisuzaki, J. Fyfe, D. Gregory, J. F. Gueremy, J. Hack, A. Harzallah, P. Inness, A. Kitoh, W. K. M. Lau, B. McAvaney, R. Madden, A. Matthews, T. N. Palmer, C. K. Park, D. Randall, and N. Renno, 1996: Intraseasonal oscillations in 15 atmospheric general circulation models: Results from an AMIP diagnostic subproject. *Clim. Dynam.*, **12** (5), 325–357.
- Sperber, K. R., 2004: Madden-Julian variability in NCAR CAM2.0 and CCSM2.0. *Clim. Dynam.*, **23**, 259–278.
- Stratton, R. S., 1999: A high resolution AMIP integration using the hadley centre model hadam2b. *Clim. Dynam.*, **15** (1), 9–28.
- Taylor, K. E., D. Williamson, and F. Zwiers, 2000: The sea surface temperature and sea ice concentration boundary conditions for AMIP II simulations. Rep. 60, PCMDI, Lawrence Livermore National Laboratory, Livermore, California.
- Waliser, D. E., K. Jin, I.-S. Kang, W. F. Stern, S. D. Schubert, M. L. C. Wu, K.-M. Lau, M.-I. Lee, V. Krishnamurthy, A. Kitoh, G. A. Meehl, V. Y. Galin, V. Satyan, S. K. Mandke, G. Wu, W. Liu, and C.-K. Park, 2003: AGCM simulations of intraseasonal monsoon variability associated with the asian summer monsoon. *Clim. Dynam.*, **21**, 423–446.

- Waliser, D. E., C. Jones, J. K. Schemm, and N. E. Graham, 1999a: A statistical extended-range tropical forecast model based on the slow evolution of the Madden-Julian oscillation. *J. Climate*, **12**, 1918–1939.
- Waliser, D. E., K. M. Lau, and J. H. Kim, 1999b: The influence of coupled sea-surface temperatures on the Madden-Julian oscillation: A model perturbation experiment. *J. Atmos. Sci.*, **56**, 333–358.
- Wang, B. and H. Rui, 1990: Synoptic climatology of transient tropical intraseasonal convection anomalies. *Meteorol. Atmos. Phys.*, **44**, 43–61.
- Wang, B., P. J. Webster, and H. Teng, 2005: Antecedents and self-induction of active-break south Asian monsoon unraveled by satellites. *Geophys. Res. Lett.*, **32**, L04704.
- Wang, B. and X. Xie, 1997: A model for Boreal Summer Intraseasonal Oscillation. *J. Atmos. Sci.*, **54**, 72–86.
- Webster, P. J., E. F. Bradley, C. W. Fairall, J. S. Godfrey, P. Hacker, R. A. Houze Jr., R. Lukas, Y. Serra, J. M. Hummon, T. D. M. Lawrence, C. A. Russell, M. N. Ryan, K. Sahami, and P. Zuidema, 2002: The JASMINE pilot study. *Bull. Amer. Meteorol. Soc.*, **83**, 1603–1630.
- Webster, P. J. and C. Hoyos, 2004: Prediction of monsoon rainfall and river discharge on 15–30-day time scales. *Bull. Am. Meteorol. Soc.*, **85**, 1745–1765.
- Webster, P. J., V. O. Magaña, T. N. Palmer, J. Shukla, R. A. Tomas, M. Yanai, and T. Yasunari, 1998: Monsoons: Processes, predictability, and the prospects for prediction. *J. Geophys. Res.*, **103**, 14 451–14 510.
- Woolnough, S. J., J. M. Slingo, and B. J. Hoskins, 2000: The relationship between convection and sea surface temperatures on intraseasonal timescales. *J. Climate*, **13**, 2086–2104.
- Woolnough, S. J., F. Vitart, and M. A. Balmaseda, 2007: The role of the ocean in the Madden-Julian Oscillation: Implications for MJO prediction. *Quart. J. R. Meteorol. Soc.*, **133**, 117–128.

- Yasunari, T., 1979: Cloudiness fluctuations associated with the Northern Hemisphere summer monsoon. *J. Meteorol. Soc. Japan*, **57**, 227–242.
- Zheng, Y., D. E. Waliser, W. F. Stern, and C. Jones, 2004: The role of coupled sea surface temperatures in the simulation of the tropical intraseasonal oscillation. *J. Climate*, **17**, 4109–4134.

List of Figures

- 1 (a) The standard deviation in the June–September (JJAS) 30–70 day bandpass-filtered OS-TIA sea-surface temperatures ($^{\circ}\text{C}$) used to force the Daily ensemble, and (b) the ratio of the standard deviation shown in (a) between the forced SSTs for the two ensembles, taken as the Daily-ensemble SSTs divided by the Monthly-ensemble SSTs. In (a) black line contours show the percentage of the total variability for which the 30–70 day band accounts, with contours at 25%, 50%, and 75%. 32
- 2 (a) The ensemble-mean JJAS-mean precipitation rate (mm day^{-1}) from the Daily ensemble; (b) the climatological JJAS-mean precipitation rate (mm day^{-1}) from the IMD gridded rainfall data; (c) the difference in (a) between the Daily and Monthly ensemble, taken as the Daily minus the Monthly ensemble; (d) the ratio of the ensemble-mean standard deviation of 30–70 day bandpass-filtered JJAS precipitation, taken as the Daily ensemble divided by the Monthly ensemble. Grey (black) dots indicate statistical significance at the 5% (10%) level using an (c) two-tailed Student’s t -test and (d) a two-tailed F-test. 33
- 3 The area-averaged precipitation rate (mm day^{-1}) taken over all Indian land points ($10^{\circ}\text{--}30^{\circ}\text{N}$, $70^{\circ}\text{--}90^{\circ}\text{E}$) for (a) the Daily ensemble and (b) the Monthly ensemble for (black) the individual ensemble members and (red) the ensemble-mean. The yellow line gives the daily climatology from the all-India rainfall dataset (1901–2005); the green line gives the all-India rainfall for 2005. 34
- 4 The ensemble-mean one-dimensional wavelet transform of (a,b) area-averaged precipitation (mm day^{-1}) and (c,d) area-averaged sea-surface temperatures in the northern Bay of Bengal ($15^{\circ}\text{--}20^{\circ}\text{N}$, $85^{\circ}\text{--}90^{\circ}\text{E}$), for (left column) the Daily ensemble and (right column) the Monthly ensemble. The solid black contours indicate the 90% and 95% confidence intervals against red noise, while the dashed black contour indicates the region outside of which edge effects distort the results. 35

5	Probability density function of the intraseasonal-power metric for (solid line) the Daily ensemble, (long dash) the Monthly ensemble, and (dash-dot) the 1997–2006 1°x1°gridded, daily precipitation analyses from GPCP. The value of this metric for 2005—the year of the SST forcing—is shown as a vertical, short-dashed line.	36
6	Lag correlations between the linear trend (11-day window) in longitude-averaged (80–90°E) rainfall and SST over JJAS for (a) the Daily ensemble, (b) the Monthly ensemble, and (c) GPCP rainfall and TMI SSTs from 1998–2006. Grey shading indicates statistical significance at the 5% level.	37
7	The linear trend (11-day window) in longitude-averaged rainfall (85–90°E; mm day ⁻²) for (a) the Daily ensemble mean, (b) the Monthly ensemble mean, (c–h) three members from the (left column) Daily ensemble and (right column) Monthly column with values of the intraseasonal-power metric closest to the most-probable value for the respective ensemble, and (i) the GPCP analysis for 2005. Note that (a) and (b) have smaller contour intervals than the other panels.	38
8	As in Figure 7, but for lead-lag correlations of 30–50 day bandpass-filtered longitude-averaged rainfall (85–90°E), with the base point at 20°N. Contours are drawn every 0.2, with negative contours dashed and the zero contour line omitted. Grey shading indicates statistical significance at the 5% level.	39
9	As in Figure 7, but for the three members from (left column) the Daily ensemble and (right column) the Monthly ensemble with the value of the intraseasonal-power metric closest to the value for the 2005 GPCP analysis.	40
10	As in Figure 8, but for the “observational members” shown in Figure 9.	41

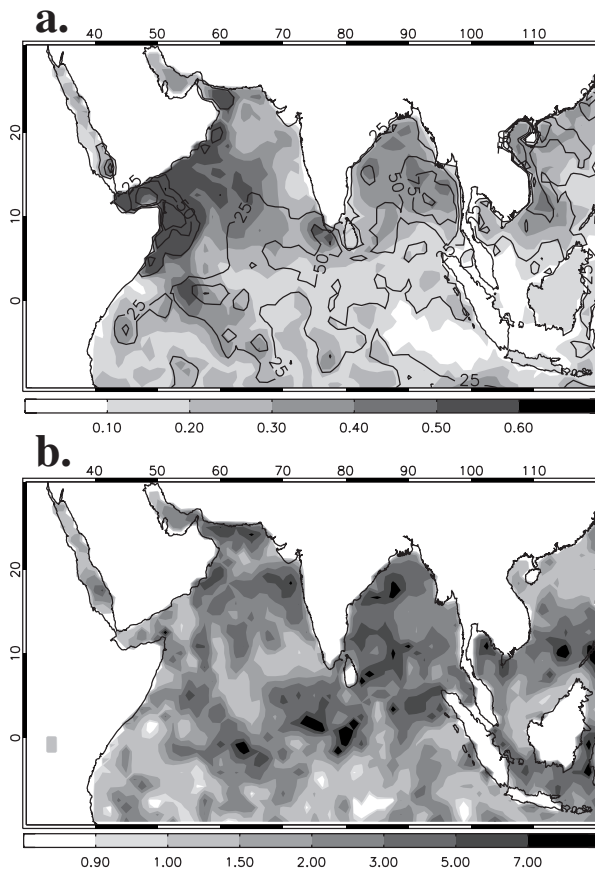


Figure 1: (a) The standard deviation in the June–September (JJAS) 30–70 day bandpass-filtered OSTIA sea-surface temperatures (°C) used to force the Daily ensemble, and (b) the ratio of the standard deviation shown in (a) between the forced SSTs for the two ensembles, taken as the Daily-ensemble SSTs divided by the Monthly-ensemble SSTs. In (a) black line contours show the percentage of the total variability for which the 30–70 day band accounts, with contours at 25%, 50%, and 75%.

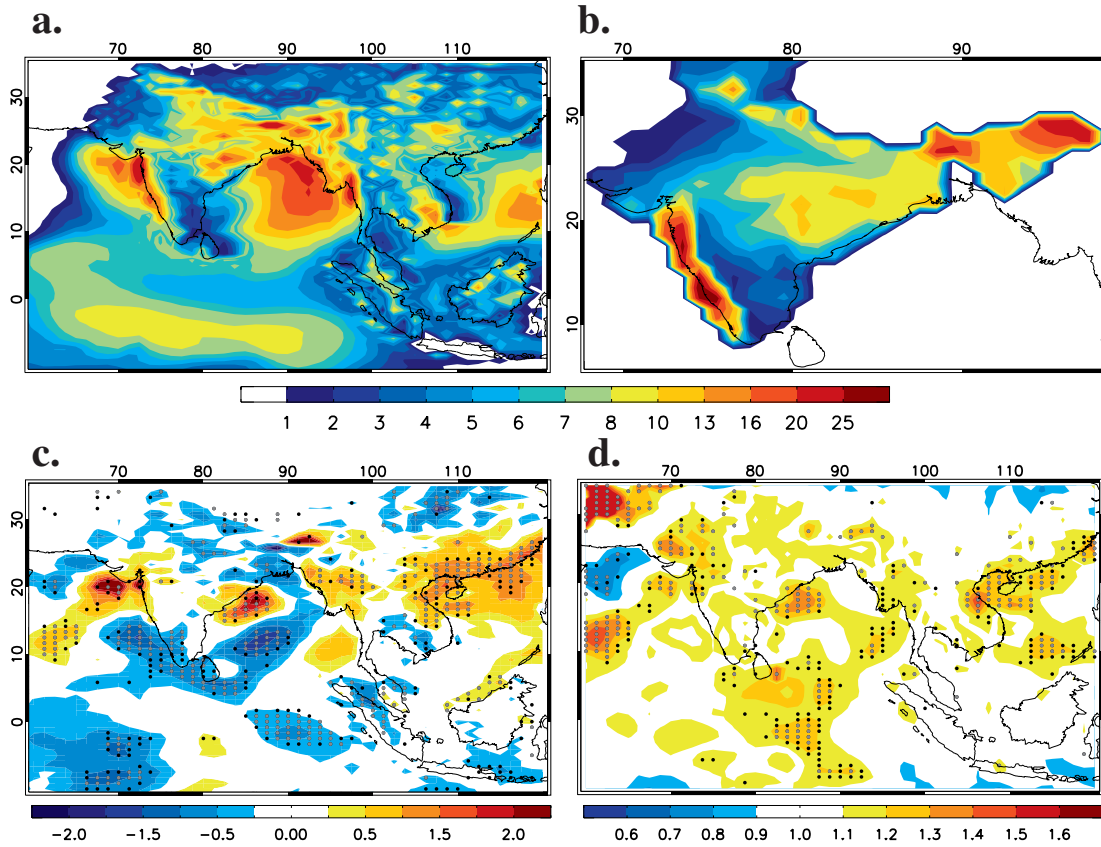


Figure 2: (a) The ensemble-mean JJAS-mean precipitation rate (mm day^{-1}) from the Daily ensemble; (b) the climatological JJAS-mean precipitation rate (mm day^{-1}) from the IMD gridded rainfall data; (c) the difference in (a) between the Daily and Monthly ensemble, taken as the Daily minus the Monthly ensemble; (d) the ratio of the ensemble-mean standard deviation of 30–70 day bandpass-filtered JJAS precipitation, taken as the Daily ensemble divided by the Monthly ensemble. Grey (black) dots indicate statistical significance at the 5% (10%) level using an (c) two-tailed Student's t -test and (d) a two-tailed F-test.

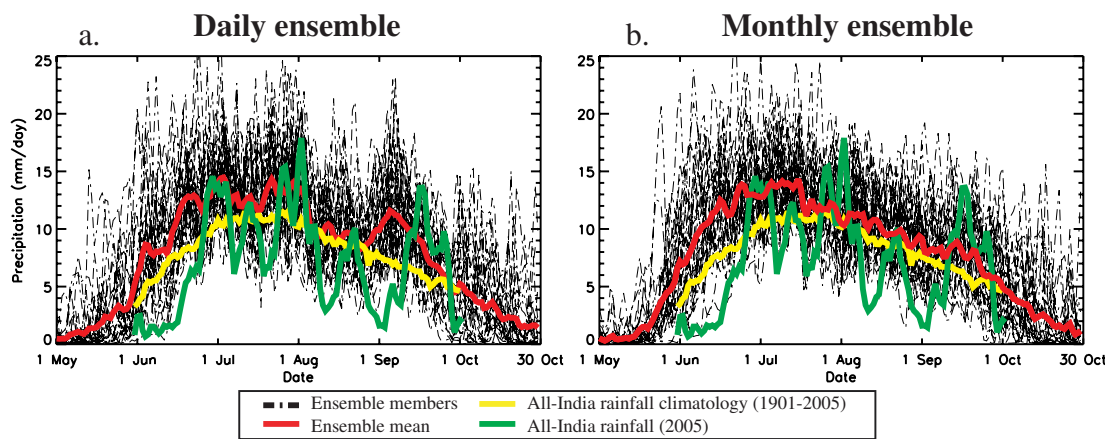


Figure 3: The area-averaged precipitation rate (mm day^{-1}) taken over all Indian land points ($10\text{--}30^\circ\text{N}$, $70\text{--}90^\circ\text{E}$) for (a) the Daily ensemble and (b) the Monthly ensemble for (black) the individual ensemble members and (red) the ensemble-mean. The yellow line gives the daily climatology from the all-India rainfall dataset (1901–2005); the green line gives the all-India rainfall for 2005.

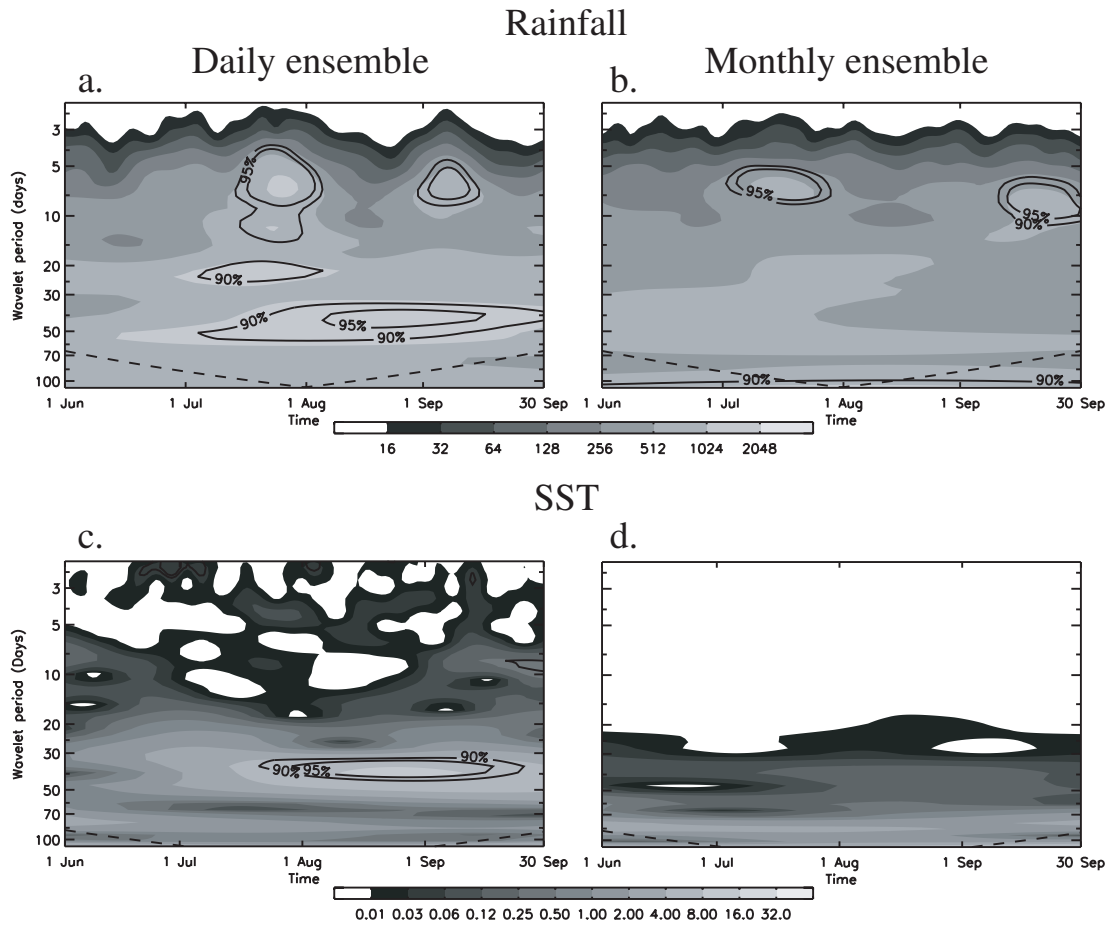


Figure 4: The ensemble-mean one-dimensional wavelet transform of (a,b) area-averaged precipitation (mm day^{-1}) and (c,d) area-averaged sea-surface temperatures in the northern Bay of Bengal (15° – 20° N, 85° – 90° E), for (left column) the Daily ensemble and (right column) the Monthly ensemble. The solid black contours indicate the 90% and 95% confidence intervals against red noise, while the dashed black contour indicates the region outside of which edge effects distort the results.

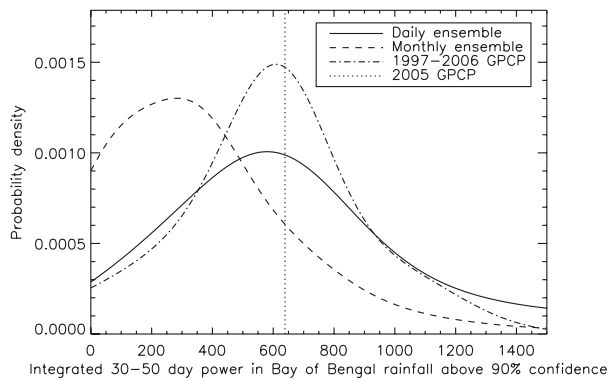


Figure 5: Probability density function of the intraseasonal-power metric for (solid line) the Daily ensemble, (long dash) the Monthly ensemble, and (dash-dot) the 1997–2006 $1^\circ \times 1^\circ$ gridded, daily precipitation analyses from GPCP. The value of this metric for 2005—the year of the SST forcing—is shown as a vertical, short-dashed line.

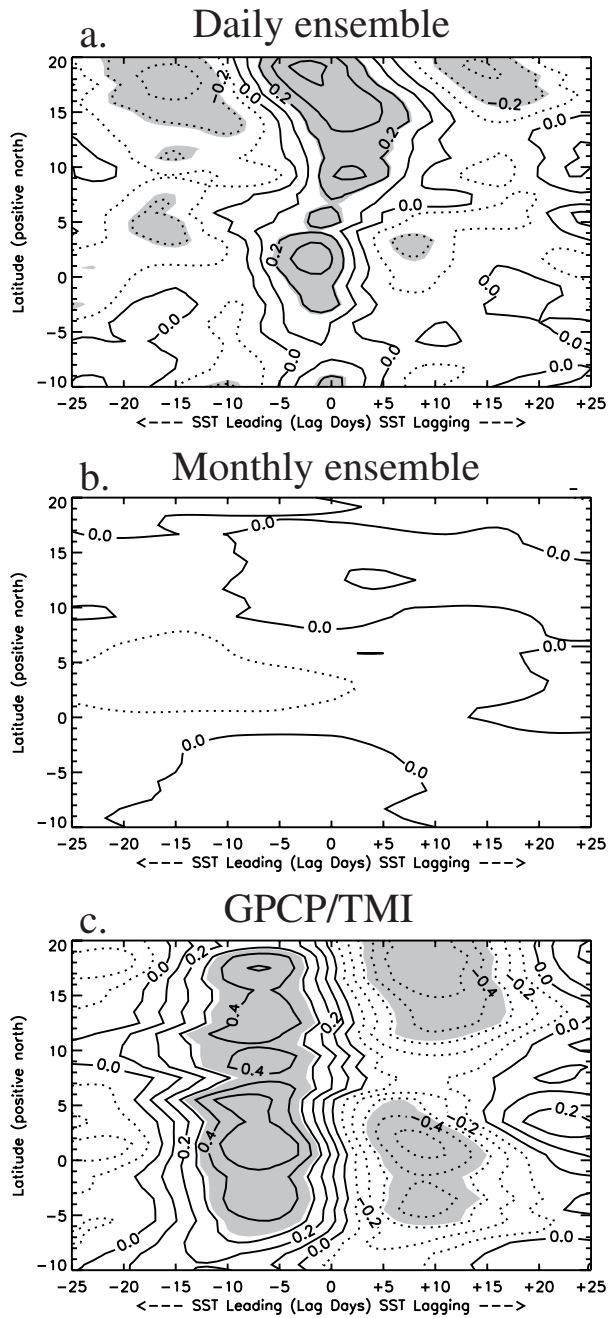


Figure 6: Lag correlations between the linear trend (11-day window) in longitude-averaged (80–90°E) rainfall and SST over JJAS for (a) the Daily ensemble, (b) the Monthly ensemble, and (c) GPCP rainfall and TMI SSTs from 1998–2006. Grey shading indicates statistical significance at the 5% level.

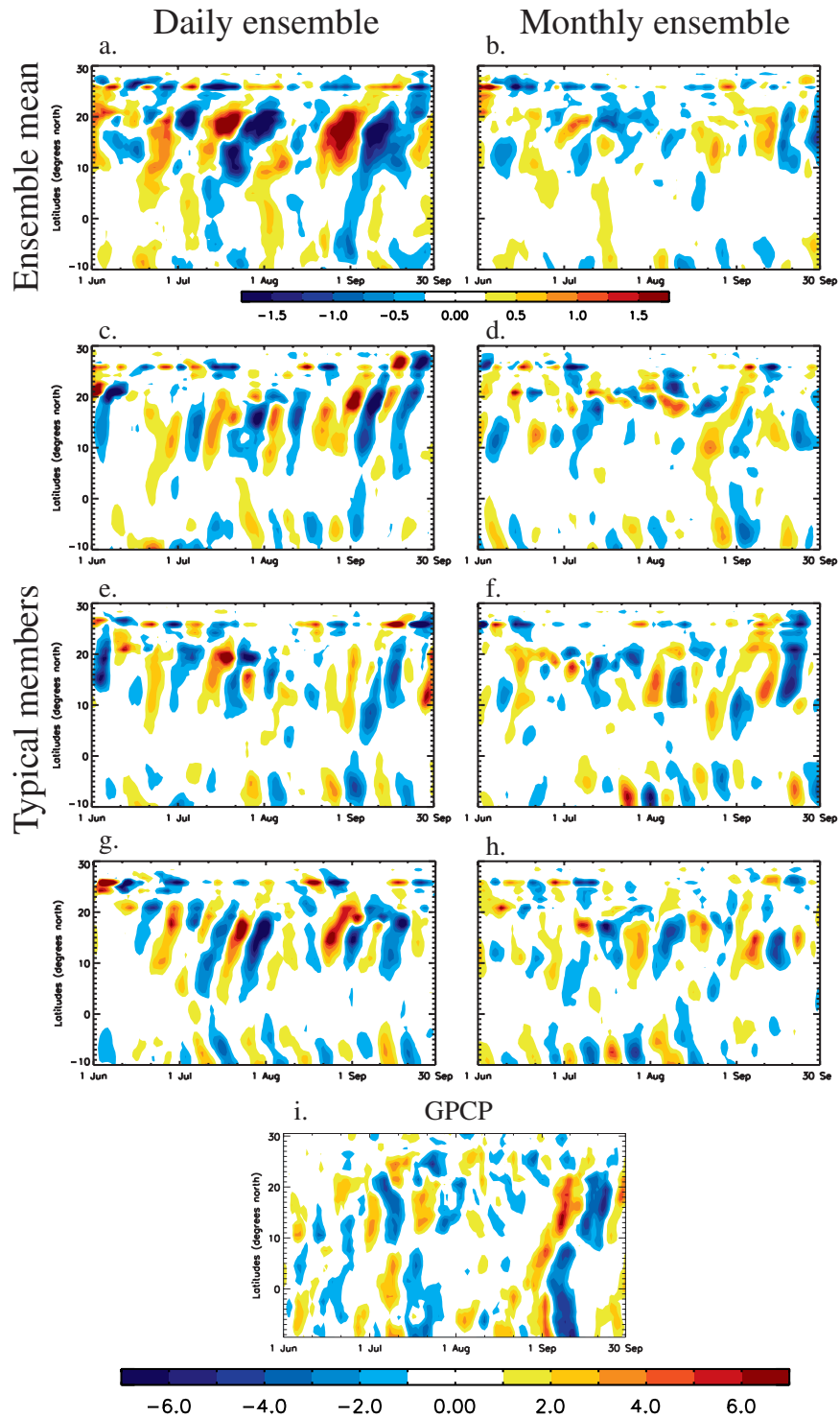


Figure 7: The linear trend (11-day window) in longitude-averaged rainfall ($85\text{--}90^\circ\text{E}$; mm day^{-2}) for (a) the Daily ensemble mean, (b) the Monthly ensemble mean, (c–h) three members from the (left column) Daily ensemble and (right column) Monthly column with values of the intraseasonal-power metric closest to the most-probable value for the respective ensemble, and (i) the GPCP analysis for 2005. Note that (a) and (b) have smaller contour intervals than the other panels.

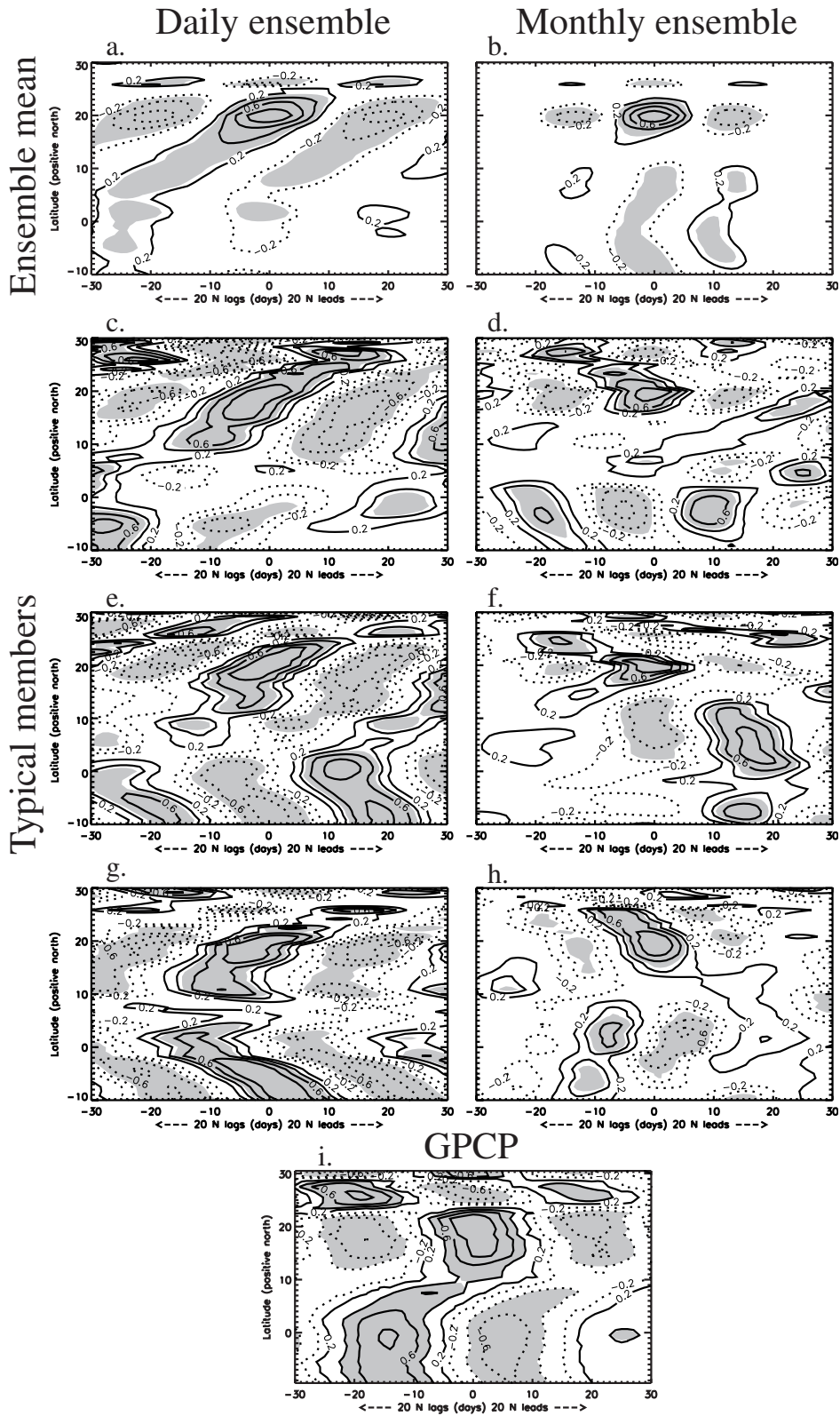


Figure 8: As in Figure 7, but for lead-lag correlations of 30–50 day bandpass-filtered longitude-averaged rainfall (85–90°E), with the base point at 20°N. Contours are drawn every 0.2, with negative contours dashed and the zero contour line omitted. Grey shading indicates statistical significance at the 5% level.

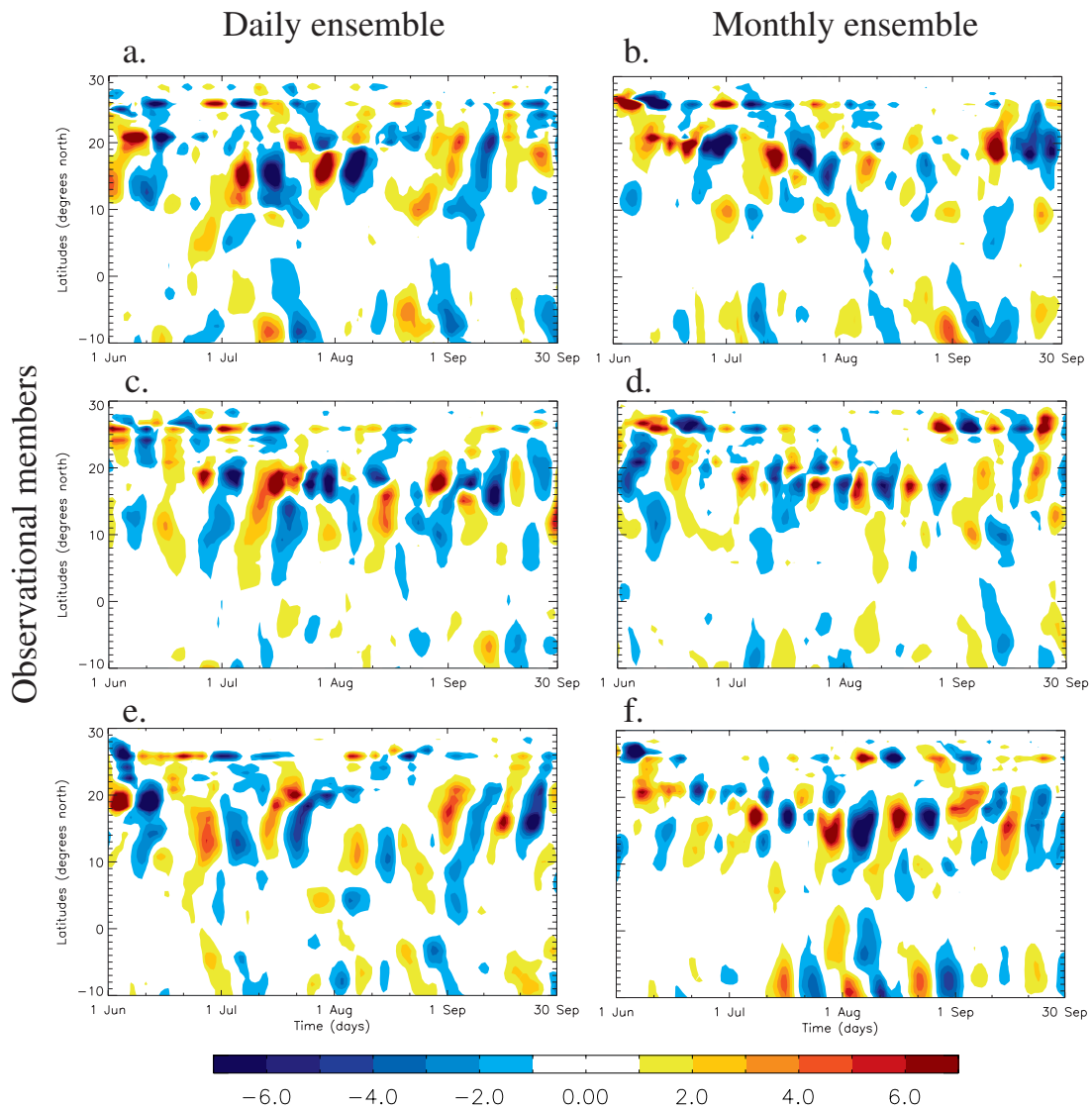


Figure 9: As in Figure 7, but for the three members from (left column) the Daily ensemble and (right column) the Monthly ensemble with the value of the intraseasonal-power metric closest to the value for the 2005 GPCP analysis.

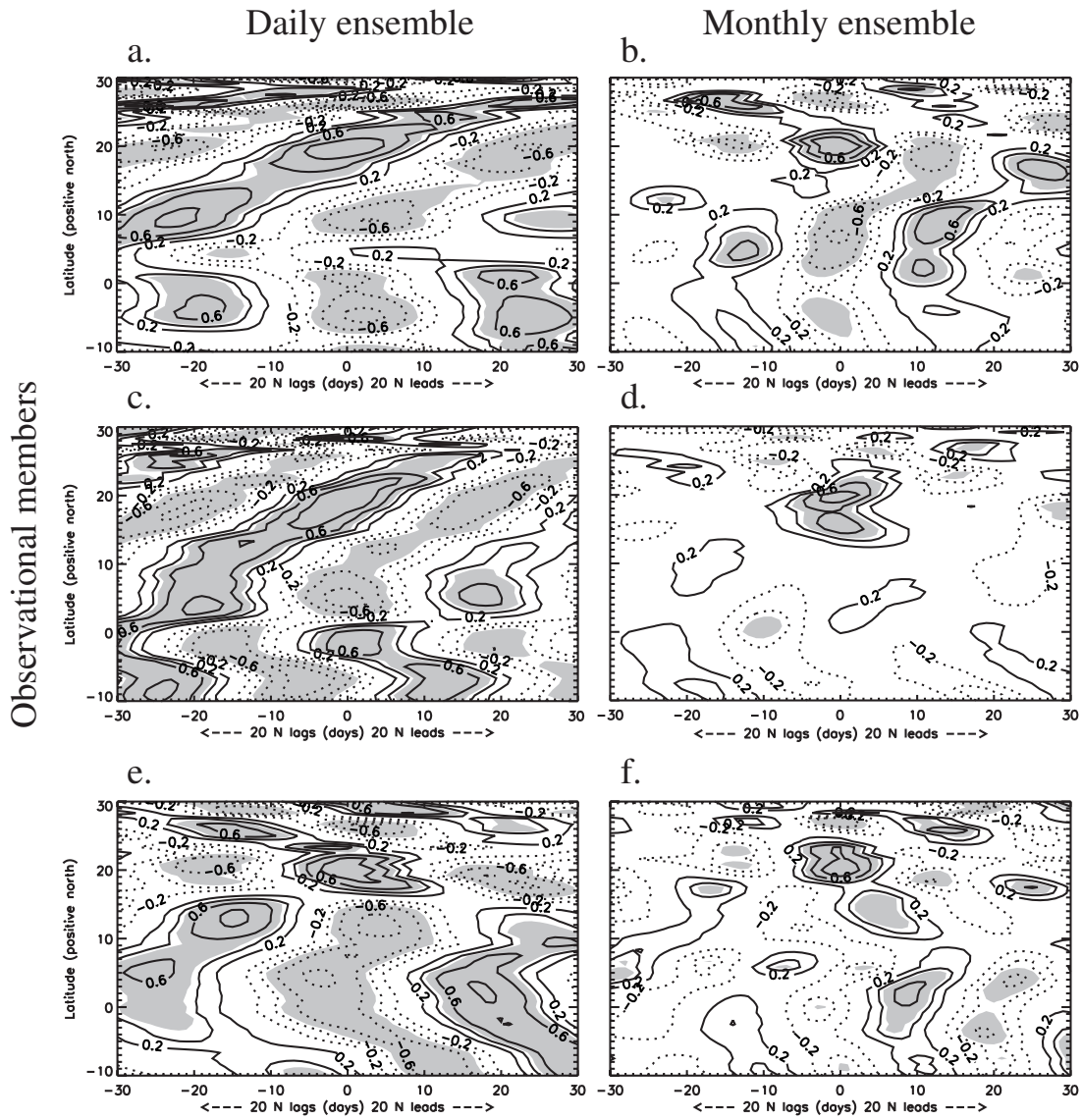


Figure 10: As in Figure 8, but for the “observational members” shown in Figure 9.